Proceedings of the ASME 2015 International Conference and Exhibition on Packaging and Integration of Electronic and Photonic Microsystems and ASME 2015 International Conference on Nanochannels, Microchannels, and Minichannels
InterPACKICNMM2015
July 6-9, 2015, San Francisco, CA, USA

InterPACKICNMM2015-48670

COMPUTATIONAL MODELING OF EXTREME HEAT FLUX MICROCOOLER FOR GaN-BASED HEMT

Hyoungsoon Lee
Stanford University
Stanford, CA, USA

Yoonjin Won
Stanford University
Stanford, CA, USA

Farzad Houshmand
Stanford University
Stanford, CA, USA

Catherine Gorle[1]
Stanford University
Stanford, CA, USA

Mehdi Asheghi
Stanford University
Stanford, CA, USA

Kenneth E. Goodson
Stanford University
Stanford, CA, USA

ABSTRACT

This study explores an extreme heat flux limit of microcooler for GaN-based HEMTs (high electron mobile transistors) which have local power densities exceeding 30 kW/cm^2 using both solid conduction simulation and single-phase/two-phase conjugate simulations. Solid conduction simulation models are developed for full geometry of the microcooler to account for the overall thermal resistances from GaN HEMT to working fluid. This allows investigating the temperature distribution of the suggested microcooler. Parametric studies are also performed to investigate the impact of geometries and heat transfer coefficients on the junction temperature. The solid conduction simulation results using COMSOL Multiphysics agree well with single-cell ANSYS Fluent simulation results.

Separately, fluid-solid conjugate CFD (Computational Fluid Dynamics) simulation models provide the detailed flow information in the microchannel using a single-channel geometry with symmetry boundary conditions. Single-phase CFD simulations obtain the lower bound of total pressure drop and heat transfer coefficient at the microchannel walls for a mass velocity range of G = 6000 – 24000 kg/m^2-s. The local temperatures and velocity distributions are reported that can help with identifying the locations of the maximum velocity and recirculation regions that are susceptible to dryouts. Two additional alternative tapered inlet designs are proposed to alleviate the significant pressure loss at the entrance of the SiC channel. The impact of the tapered inlet designs on pressure drops and heat transfer coefficients is also investigated.

Two-phase simulations in microchannel are conducted using Volume-of-Fluid (VOF) method embedded in ANSYS Fluent to investigate two-phase flow patterns, flow boiling, and temperature distributions within the GaN HEMT device and SiC etched mircochannels. A user-defined function (UDF) accounts for the phase change process due to boiling at the microchannel walls. The results show that the time relaxation factor, r_i has a strongly influence on both numerical convergence and flow solutions.

INTRODUCTION

Thermal managements of the extreme heat flux devices such as power electronics, avionics, lasers, and X-ray are always the most challenging issue as demands of integration density and power dissipation are increased. Microchannel heat sinks have been widely utilized to achieve the high flux cooling since the pioneer work by Tuckerman and Pease in the early 1980's [1,2]. Over the last decades, microchannel heat sinks have been significantly improved with innovations of microfluidics geometries with advanced manufacturing techniques such as micro-scale structure fabrications and 3D manifolding [3,4]. As geometric complexity increases, numerical approaches have been a prime role to reduce design cost and uncertainty as well as to assist with better understanding of the flow physics.

Present study explores cooling solutions for the extreme heat flux multichannel microcooler module which dissipates up to 30 kW/cm^2 at the device footprint. Two different approaches are performed to investigate thermo-fluid design point of the microcooler: 1) Solid conduction simulation models using COMSOL Multiphysics are developed to account

[1] Current affiliation: Department of Civil Engineering and Engineering Mechanics, Columbia University, New York, NY, 10027

for the overall thermal resistances from GaN HEMT to working fluid. Extensive and exhausting literature survey of the existing flow boiling heat transfer correlations along with novel experimental tests at extreme heat flux (1-3 kW/cm^2) conditions have been conducted to find an appropriate range of heat transfer coefficients in a wide range of channel sizes. 2) In addition, single and two-phase conjugate CFD simulations are conducted using ANSYS Fluent to obtain the much needed insight on the details of flow patterns, local heat transfer coefficients and heat flux values as well as pressure drops in various segments of the flow channel.

SOLID CONDUCTION SIMULATION

Geometry description for solid conduction simulation

A solid conduction simulation is performed using COMSOL Multiphysics to account for the thermal resistances associated with the GaN, SiC substrates, and SiC channels for the full chip microcooler. As shown in Figure 1, the GaN has 40 multiple gates of 2 µm × 350 µm. A 1.5 µm-thick GaN layer is located underneath of the gates and a 10 µm-thick SiC layer is attached to improve the heat spreading. The following structure is 90 µm-deep SiC channels by assuming that 90 µm-deep channel etching is feasible with 9:1 aspect ratio by using inductive coupled plasma etching technique [5].

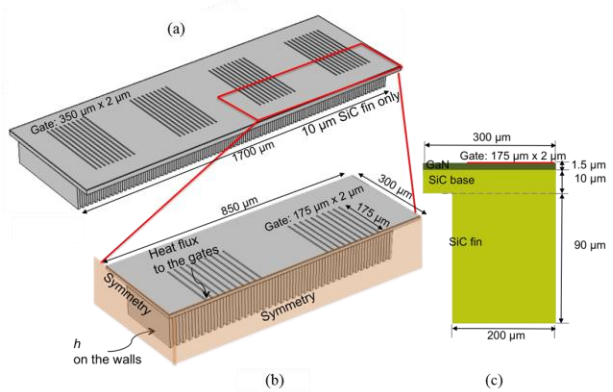

Figure 1 3D view of (a) the system level device, (b) quarter symmetry device. (c) Cross-sectional view of the microchannel, which shows a 1.5 µm-thick GaN layer, 10 µm-thick SiC base, and 90 µm-thick SiC channel.

COMSOL Multiphysics is used to examine each thermal resistance and temperature rise between the junction and the fin walls by solving for the temperature field as the solution to the steady state heat conduction equation below.

$$-n\cdot\left(-k\nabla T\right)=q''. \qquad (1)$$

where k is the thermal conductivity of each layer and T is the temperature.

Boundary conditions

The total power of 92.4 W is applied to the gates resulting in the heat flux of 330 kW/cm^2 to the gates and 30 kW/cm^2 to 350 µm × 220 µm footprint. A range of heat transfer coefficients is imposed to the fin walls as an independent variable in order to investigate its impact on the maximum junction temperature. The range is selected based on the relevant two-phase correlations as well as single-phase simulation results (See following section). Symmetric conditions are assigned to two surfaces of the quarter symmetry device as shown in Figure 1(b). The other surfaces are considered as adiabatic. The simulation models include the properties and dimensions of each layer. The models account for the thermal conductivity of GaN and SiC as a function of temperature as indicated in Table 1.

Table 1 Thermodynamic properties used in the study

Methanol		
	liquid	**vapor**
ρ	742.8 kg/m^3	1.5 kg/m^3
C_p	2520 J/kg-K	4536 J/kg-K
k	0.2011 W/m-K	0.0209 W/m-K
μ	30.62×10^{-5} kg/m-s	1.1×10^{-5} kg/m-s
h_{fg}	1090.1 kJ/kg	
SiC		
k	0.0038 T^2 - 4.1734 T + 1259 W/m-K, T (in K)	
GaN		
k	-0.1623 T+ 214.17 W/m-K, T (in K)	

Investigation of relevant flow boiling heat transfer coefficient ranges from the literature

There are numerous predictive flow boiling heat transfer correlations available in the literature. Thus, it is important to investigate the valid application ranges of important parameters and dominant heat transfer mechanisms [6]. Figure 2 shows the ranges of hydraulic diameters and mass fluxes for the relevant correlations, the microtube experiment, and the present microcooler device as well. The solid lines are for the correlations developed based on experimental data using a single type of working fluid while the dashed lines are for the correlations developed based on a consolidated database using more than two different working fluids. It should be highlighted that the hydraulic diameter of the present microcooler device is more than two orders of magnitude smaller compared to those of the selected correlations in the similar mass flux ranges. Thus, we select four different two-phase boiling correlations based on hydraulic diameter and mass flux ranges close to our design and the additional microtube experiment is conducted to validate those correlations in the smaller hydraulic diameters with the relatively high heat flux ranges [7]. Kim and Mudawar [8], and Bertsch et al.[16] are universal correlations based on wide ranges of mass flux, hydraulic diameter, heat transfer coefficient, and heat flux. Cioncolini and Thome [12] correlation is used to calculate heat transfer coefficient specifically for annular flow dominant regime due to the early transition from the coalescing bubble flow regime to the annular flow regime in relatively smaller hydraulic diameter channels. For the present microcooler geometry, the transition

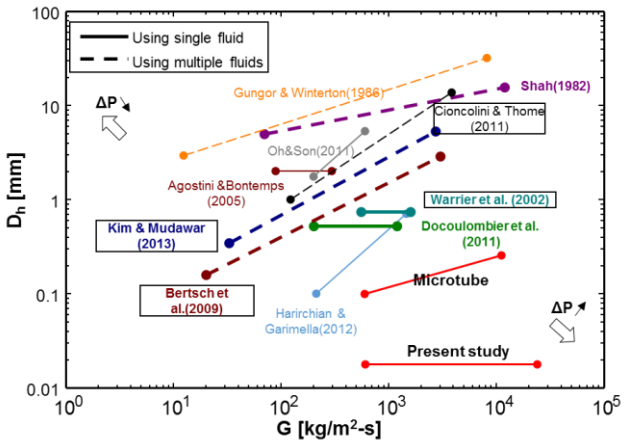

Figure 2 Hydraulic diameter and mass velocity ranges for various correlations.

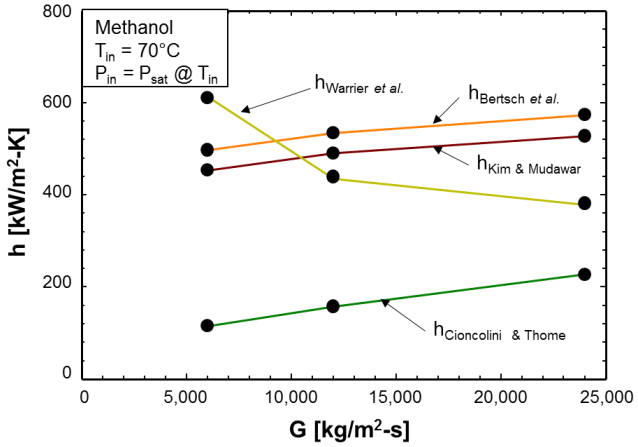

Figure 3 Heat transfer coefficients for three different mass fluxes of G = 6000, 12000 and 24000 kg/m^2-s obtained from four different correlations.

to annular flow happens at the vapor quality of x = 0.057 – 0.012 for G = 6000 – 24000 kg/m^2-s based on Costa-Patry and Thome [18] correlation which is expressed below.

$$x_{CB-AF} = 425\left(\frac{\rho_g}{\rho_f}\right)^{0.1}\frac{Bo^{1.1}}{Co^{0.5}}, \qquad (2)$$

Bo and Co are the boiling number $Bo = q''/(Gh_{fg})$ and the Confinement number ($Co = \sqrt{s/g(r_f - r_g)}/D_h$), respectively. Warrier *et al.*[9] correlation is also used for nucleate boiling dominant regime as a comparison.

Figure 3 shows the range of heat transfer coefficient values obtained from the selected correlations for three different mass fluxes of G = 6000, 12000 and 24000 kg/m^2-s. Warrier *et al.*[9] correlation predicts the highest heat transfer coefficient at the lowest mass flux of G = 6000 kg/m^2-s and it is decreased due to the nucleate boiling suppression as G increases. Cioncolini and Thome [12] correlation underpredicts the heat transfer coefficients compared to those from other correlations since it is based on the convective boiling data. Overall, calculated heat transfer coefficients have a range of h = 116 – 605 kW/m^2-K for mass velocities of G = 6000 – 24000 kg/m^2-s for the present microcooler design.

Junction temperature values from solid conduction simulation models

Figure 4 shows an example of solid conduction simulation results when a convective heat transfer coefficient of 400 kW/m^2-K is imposed to the fin walls. Color legend indicates the temperature distribution of the quarter symmetry device, top surface, and fin surface. For the details of temperature distribution, the temperature profile along the x-direction at the top surface and the z-direction below the hotspot are plotted in Figure 5**.** The temperature profile shown in Figure 5(a) indicates significant temperature variations and as much as ~80ºC temperature difference between the center gate and end gate. This larger temperature difference between gate locations may introduce flow instablity issues. Therefore, it is critical to improve the temperature uniformity in the future work. The temperature rise in Figure 5(b) shows the contribution of each

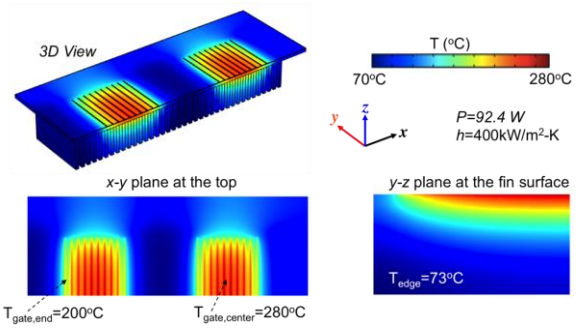

Figure 4 Temperature distributions of the quarter symmetry device, top surface, and fin side surface when a h of 400 kW/m^2-K is imposed to the fin walls.

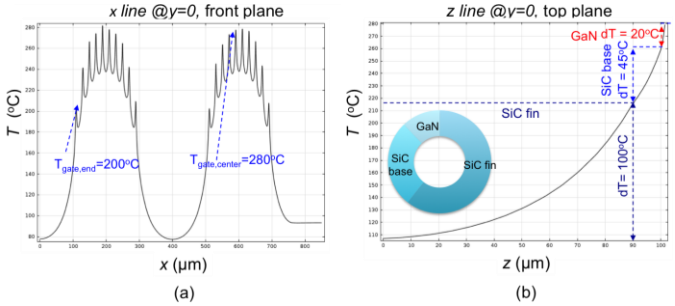

Figure 5 (a) Temperature profile along the x-direction at the top surface. (b) Temperature rise along the z-direction below the hotspot. Note that the dominant temperature rise is from SiC fins.

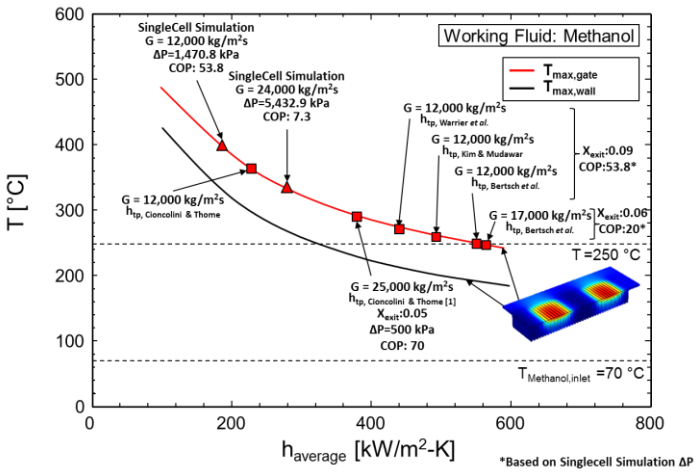

Figure 6 Junction temperature at gates and the maximum wall temperature below gates with varying convective heat transfer coefficients.

layer to the total thermal resistance from the junction to the cooling fluid. The results using a *h* of 400 kW/m^2-K shows the *dT* of 100°C, 45°C, and 20°C from SiC fins, SiC base, and GaN layer, respectively. Thus, more efficient operating condition associated with higher heat transfer coefficients can decrease the thermal resistance of SiC fins and consequently decrease the junction temperature.

The maximum junction temperature and maximum wall temperature at the fin base are plotted as increasing heat transfer coefficients in Figure 6. The red solid line indicating the junction temperature from the solid simulation models is compared to the results from both the relevant heat transfer correlations(□) and single-phase conjugate CFD models(Δ) in the following section. The junction temperature is limited by the overall thermal resistances from the GaN to the convecting fluid. Since GaN HEMT performance rapidly degrades with higher junction temperatures, the junction temperature decides the efficiency of GaN HEMT device. Therefore, one of thermal challenges is to maintain the junction temperature lower than the target junction temperature of 250°C to avoid inefficient operating ranges. The conduction simulation models estimate the junction temperature from 250-350°C with varying *h* of 200-600 kW/m^2-K. Also, the simulation models estimate the maximum wall temperature, which decides the quality level of working fluid and resulting thermofluidic performance of microcooler (*i.e.* pressure drop, COP, *etc*). For example, the models predict the maximum wall temperature from 200-300°C with varying *h* of 200-600 kW/m^2-K while the suggested working fluid, methanol has the saturation temperature as 70°C. Higher heat transfer coefficients associated with higher mass fluxes decrease the junction temperatures but increase the pressure drop as well. Therefore, we should carefully decide operating conditions to have a balance between the thermal performances and fluidic requirements.

CONJUGATE CFD SIMULATIONS

The single-phase and two-phase CFD simulations are performed for a single microchannel of the microcooler to investigate valuable details and insight on the flow patterns, local heat transfer coefficients and heat flux values as well as pressure drops in various segments of the microcooler. Single-phase CFD simulations provide the lower bound for heat transfer coefficient and pressure drop for a mass flux range of G = 6000-24000 kg/m^2-s. Two-phase boiling CFD simulations are also performed for the single microchannel using a Lee model [19], which is the most widely used for phase change process, to provide both flow regimes and local temperature solutions which are important to utilize available two-phase boiling heat transfer correlations.

Computational domain and governing equations for single-phase conjugate CFD model

A single microchannel from the present microcooler design is computationally investigated as shown in Figure 7. A three-dimensional computational domain with symmetry boundary conditions applied for all front, back and inlet side walls is used for the single-phase conjugate simulation. The gate has a 2 × 175 μm^2 area with a 1-μm thickness. A 1.5-μm GaN-substrate and a 10-μm thickness SiC are located right underneath of the gate. A 10-μm × a 90-μm single microchannel is constructed using a 5-μm thickness SiC fins beneath of the 10-μm SiC substrate. Methanol enters the single-cell through the bottom right inlet. After flowing through a 127-μm of inlet delivery line, it is introduced to the microchannel and exited towards to the bottom left. Three different inlet designs are tested to investigate the effect of pressure drop and heat transfer coefficient as illustrated in Figure 7(a) and (b). ANSYS Fluent is used to compute the conservation equations of the single-cell simulation and the governing equations are expressed as below[20].

Continuity:
$$\frac{\partial}{\partial t}(\rho)+\nabla\cdot(\rho\vec{u})=0\,, \qquad (3)$$

Momentum:
$$\frac{\partial}{\partial t}(\rho\vec{u})+\nabla\cdot(\rho\vec{u}\vec{u})=-\nabla P+\nabla\cdot\left[\mu\left(\nabla\vec{u}+\nabla\vec{u}^{T}\right)\right]+\rho\vec{g}+\vec{F}\,, \qquad (4)$$

Energy:
$$\frac{\partial}{\partial t}(\rho E)+\nabla\cdot\left(\vec{u}(\rho E+P)\right)=\nabla\cdot(k\nabla T)+Q\,. \qquad (5)$$

Hexahedral mesh is used for the fluid domain and combination of hexahedral and tetrahedral meshes are applied for the solid domain of different inlet geometries as shown in Figure 7. Approximately total one million cells are used for the no tapered and the two different 45° tapered designs. Figure 8 shows the averaged heat transfer coefficient and wall temperature at the microchannel walls for different mesh sizes in the fluid domain for the mesh dependency. As shown in the figure, both the averaged heat transfer coefficient and wall temperature reach asymptotic values below a cell (mesh)

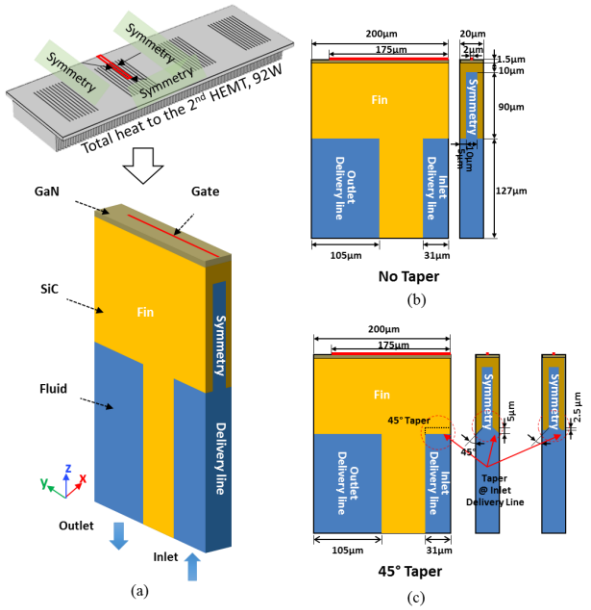

Figure 7 (a) Construction of single-cell computational model, (b) Front and side view for no tapered model and (c) Front and side view for two different 45° tapered models.

volume of 3.3 μm^3 for the mass fluxes up to 12000 kg/m^2-s and the finer mesh is needed for the higher mass fluxes than G = 12000 kg/m^2-s. In this study, the cell sizes of 1-μm are adopted in the fluid domain to minimize computation efforts.

The single-phase single-cell is simulated using pressure-based solver. Turbulence effects are taken into account using the standard two-equation k-ε turbulent model as prescribed in the ANSYS Guide [20] and Semi-Implicit Method for Pressure-Linked Equations (SIMPLE) is used to tackle pressure-velocity coupling. The PREssure STaggering Option (PRESTO) and the third-order Monotonic Upstream-centered Scheme for Conservation Laws (MUSCL) [23] are used for pressure and momentum discretization, respectively. The first-order upwind scheme is adopted [24] for both turbulent kinetic energy and specific dissipation rate, and second-order upwind scheme [24] used for energy discretization.

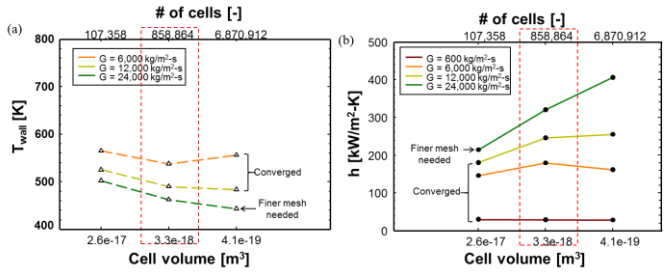

Figure 8 Average wall temperature and heat transfer coefficient for different mesh sizes.

Single-phase CFD simulation results and discussion

Figure 9(a-c) show the computed heat transfer coefficients at the microchannel walls for three different mass fluxes of G = 6000, 12000 and 24000 kg/m^2-s, respectively. As shown in these figures, the heat transfer coefficient is relatively high at the inlet of microchannel where the local velocities are the highest due to the sudden contraction at the entrance. And it is also higher at the center of the top channel walls due to the jet impingement effect. The higher heat transfer coefficient at the top wall due to the jet impingement is more dominant as G increases.

Figure 10(a) and (b) show the computed pressure drop results for two different mass fluxes of G = 6000 and 24000 kg/m^2-s. It should be noted that almost 50% of the entire pressure drop occurs at the entrance of microchannel due to the sudden contraction. Therefore, the 45° tapered designs shown in Figure 7(c) are also tested to alleviate the entrance effect . The total pressure drops for the tapered designs are significantly reduced compared to those of the no-tapered design with negligible changes of the heat transfer coefficient. The heat transfer coefficient and the pressure drop comparisons for different mass fluxes between the no-tapered and the 45° tapered designs are shown in Figure 11.

Temperature and velocity contour plots are also obtained to explore the maximum temperature and velocity in the computational domain. Figure 12 illustrates the computed temperature contour plots for the three different mass fluxes at the fin surface, the center-plane of the microchannel, and the top surface of the GaN substrate. The maximum hot spot

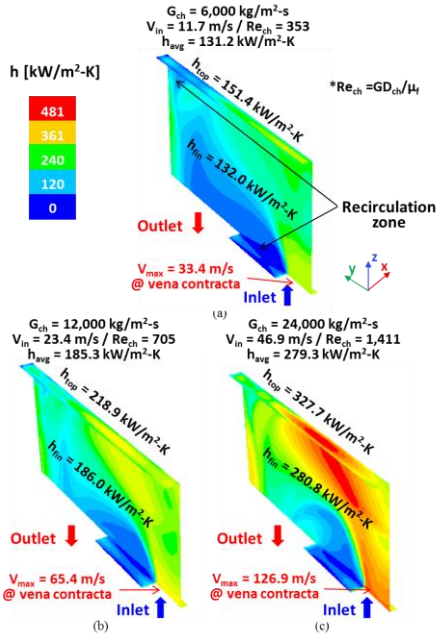

Figure 9 Computed heat transfer coefficient contours for three different mass fluxes of (a) G = 6000 kg/m^2-s, (b) G = 12000 kg/m^2-s, and (c) G = 24000 kg/m^2-s.

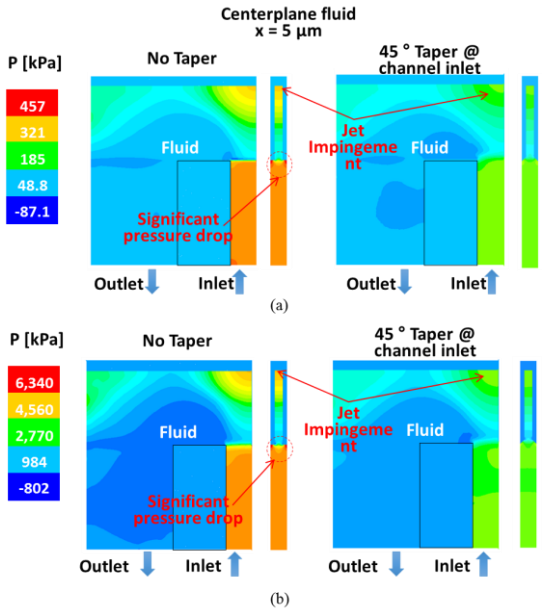

Figure 10 Computed pressure contours of no tapered and 45° tapered designs for two different mass fluxes of (a) G = 6000 kg/m^2-s, and (b) G = 24000 kg/m^2-s.

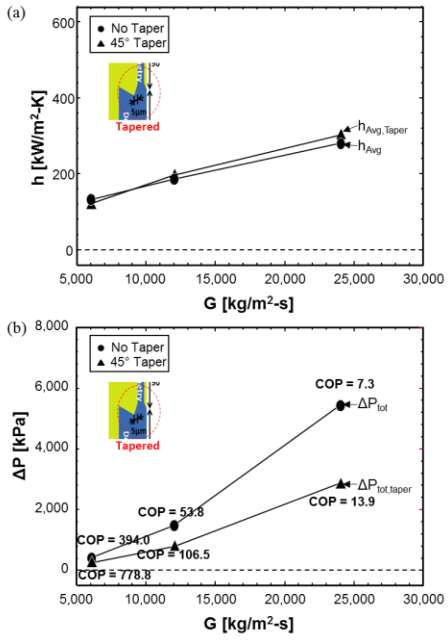

Figure 11 (a) Averaged heat transfer coefficient and (b) pressure drop of three different mass fluxes of G = 6000, 12000, and 24000 kg/m^2-s for two different inlet designs.

temperature located at the gate varies from 461°C for G = 6000 kg/m^2-s to 333°C for G = 24000 kg/m^2-s. The corresponding maximum wall temperature at the microchannel also decreases from 387°C to 259°C as mass flux increases from G = 6000 to

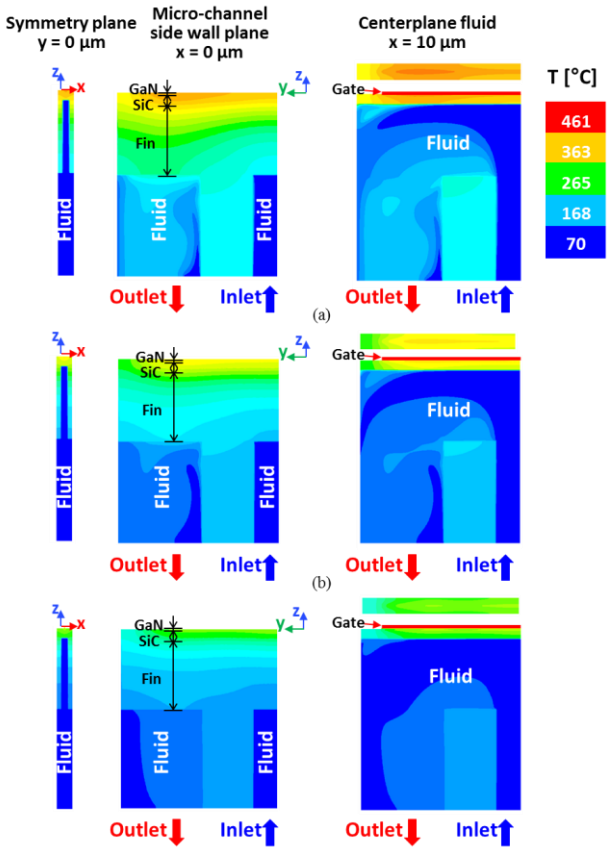

Figure 12 Computed temperature contours for three different mass fluxes of (a) G = 6000 kg/m^2-s, (b) G = 12000 kg/m^2-s, and (c) G = 24000 kg/m^2-s.

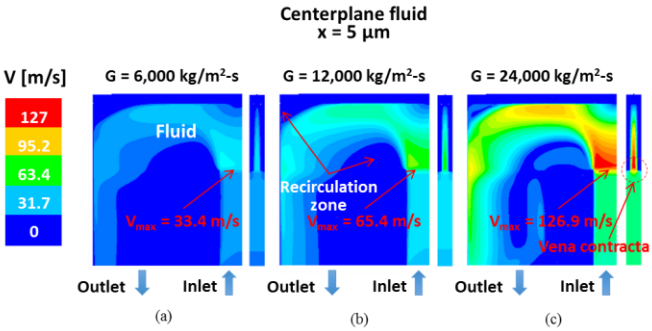

Figure 13 Computed velocity contours for three different mass fluxes of (a) G = 6000 kg/ m^2-s, (b) G = 12000 kg/ m^2-s, and (c) G = 24000 kg/ m^2-s.

24000 kg/m^2-s. Figure 13 has velocity contour at the centerline of microchannel and the symmetry inlet side plane for the no-tapered design. The maximum velocity always occurs at the vena contracta of the channel entrance and it varies from 33.4 m/s to 126.9 m/s. The single-cell simulation results are summarized in Table 2 and Table 3

Table 2 Single-cell simulation results

G [kg/m²s]	h_{avg}	T_{max} @gate	T_{avg} @gate	T_{max} @TopGaN	T_{avg} @TopGaN	T_{max} @TopCh	T_{avg} @TopCh	V_{max}	ΔP_{total}	$\Delta P_{total,}$ Taper	COP No Taper	COP Taper
6000	131.3	461	448	423	383	387	368	33.4	402	203	394	789
12000	185.3	398	390	364	324	323	306	65.4	1471	743	53.8	107
24000	279.3	333	324	302	261	259	242	127	5433	2,845	7.3	13.9

Table 3 Pressure drops through the single-cell for three different inlet tapered designs

G [kg/m²s]	ΔP [kPa]		
	No Taper	**45° Taper 1**	**45° Taper 2**
6000	**402**	**203**	**250**
12000	**1,471**	**743**	**848**
24000	**5,433**	**2,845**	**3,987**

Computational domain and governing equations for two-phase boiling simulation

As shown earlier in Figure 12, the microchannel wall temperatures obtained from the single-phase single-cell simulations are higher than the saturated temperature and localized incipient of boiling may occur at the heated walls. Therefore, two-phase boiling simulation is performed using the single-cell computational domain to investigate flow features under the extreme operating condition of the current microcooler design. Obtained flow information gives useful information for both flow regimes and heat transfer coefficient study which are important to utilize available correlations.

The VOF method [25] adopted in Fluent is used to compute the conservation equations for liquid and vapor while also accounting for mass transfer between phases using Lee model [19] which is expressed as following equations:

$$S_g = -S_f = r_i \alpha_g \rho_g \frac{(T - T_{sat})}{T_{sat}} \quad \text{for condensation } (T < T_{sat}) \qquad (6a)$$

and

$$S_g = -S_f = r_i \alpha_f \rho_f \frac{(T - T_{sat})}{T_{sat}} \quad \text{for evaporation } (T > T_{sat}), \qquad (6b)$$

The continuity equations are expressed as[22]

liquid phase: $$\frac{\partial}{\partial t}(\alpha_f \rho_f) + \nabla \cdot (\alpha_f \rho_f \vec{u}_f) = S_f , \qquad (7a)$$

vapor phase: $$\frac{\partial}{\partial t}(\alpha_g \rho_g) + \nabla \cdot (\alpha_g \rho_g \vec{u}_g) = S_g . \qquad (7b)$$

The momentum and energy equations, which are written for the combined phases, are expressed, respectively, as [22]

Momentum:

$$\frac{\partial}{\partial t}(\rho \vec{u}) + \nabla \cdot (\rho \vec{u} \vec{u}) = -\nabla P + \nabla \cdot \left[\mu \left(\nabla \vec{u} + \nabla \vec{u}^T\right)\right] + \rho \vec{g} + \vec{F} , \quad (8)$$

Energy:

$$\frac{\partial}{\partial t}(\rho E) + \nabla \cdot (\vec{u}(\rho E + P)) = \nabla \cdot (k_{eff} \nabla T) + Q , \qquad (9)$$

where E [J/kg] is the energy per unit mass, which is determined from [20]

$$E = \frac{\alpha_f \rho_f E_f + \alpha_g \rho_g E_g}{\alpha_f \rho_f + \alpha_g \rho_g} , \qquad (10)$$

$$\rho = \alpha_f \rho_f + \alpha_g \rho_g , \qquad (11a)$$

$$\mu = \alpha_f \mu_f + \alpha_g \mu_g , \qquad (11b)$$

and

$$k_{eff} = \alpha_f k_f + \alpha_g k_g . \qquad (11c)$$

In the present computations, mass transfer due to condensation is accounted using the appropriate mass source terms, S_f and S_g, which can be obtained from Eqs. 6(a) and (b), and the corresponding energy transfer term can be determined from

$$Q = h_{fg} S_f . \qquad (12)$$

Both the mass source terms and the energy transfer term are employed into the Fluent using user defined function (UDF) macros separately.

The hexahedral meshes with cell sizes of Δc = 1 μm³ are used for the two-phase VOF single-cell simulation. Two additional local refined meshes near the microchannel walls are also tested not only to check the mesh dependency but also to investigate the effect of cell sizes for the interfacial temperature and the mass transfer intensity factor, r_i.

The mass flux of G = 12000 kg/m²-s is used for the VOF simulation and three different r_i values are examined in pursuit of good agreement between the interfacial temperature and the saturated temperature. Variable time stepping method with Global Courant number of 2 is used to improve convergence for transient solution.

$$Co = \frac{u \Delta t}{\Delta c} , \qquad (13)$$

where u is the local velocity vector, Δt and Δc are the time step and cell size, respectively.

The thermodynamic properties shown in Table 1 are used for the two-phase VOF simulation and the same discretization methods to the single-phase single-cell simulation are used for pressure, momentum, turbulent kinetic energy, specific dissipation rate and energy while Piecewise Linear Interface

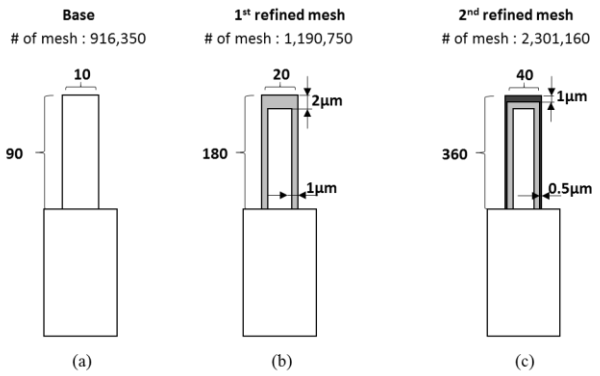

Figure 14 Three different meshes for VOF single-cell simulation.

Calculation (PLIC) algorithm (named Geo-Reconstruct in Fluent) [26] is adopted for volume fraction discretization.

A two-step solution procedure is used for the boundary condition at the hot spot area to avoid initial overheating before reaching a quasi-steady state two-phase flow solution. First, a constant temperature boundary condition is applied as the wall boundary condition at the gate, which is estimated from the solid simulation results for a range of heat transfer coefficients. Once the solution reaches a quasi-steady state using the constant temperature boundary condition, it is switched to the constant heat flux boundary condition while monitoring temperature changes at the gate and microchannel walls.

Two-phase VOF simulation results and discussions

Figure 15(a-c) shows the vapor volume fractions at the center-plane (x=5μm) for the three different mass transfer intensity factors of r_i = 10000, 20000 and 50000. As illustrated in Figure 15, r_i is not only the relaxation constant but also it actually determines how much mass is transferred due to the boiling. Therefore, determining an appropriate value for the mass transfer intensity factor, r_i, is one of the most important tasks when using the Lee model [19] for phase change simulations since this value will influence both numerical convergence and flow solutions of the entire two-phase flow field as well. Researchers have used a very wide range of r_i values and it seems to increase as computational mesh size decreases due to the developments in CPU processing speed. r_i value of 0.1 was used in very early phase change studies and relatively much higher values of r_i upto 1.0×10^7 s^{-1} were used in the recent literature [22]. Since the experimental data is not available for the current microcooler design, the temperature differences, dT, between the local temperature and the saturated temperature at the interface are examined for the three different r_i values to find appropriate r_i values which gives the minimum dT at the interface. Figure 16(a-c) compare the dT at the interface for three different values of r_i = 10000, 20000 and 50000. dT shows a wide range of dT = 2.2 – 292K in the entire fluid domain, however it should be noticed that the large dT are only found near the walls and remaining locations have relatively very low dT values such as lower than around 5K. The positive temperature difference along the entire fluid domain indicates that there are insufficient evaporation occurred especially near the heated wall since r_i value is relatively low to produce enough phase change. As r_i increases, the temperature difference is weakened along the entire fluid domain due to the increase of evaporative cooling and the minimum dT are also decreased from 5.3K to 2.2K. These results show that r_i should be allowed to vary throughout the entire computational domain to obtain a more accurate solution which is highly recommended for future study.

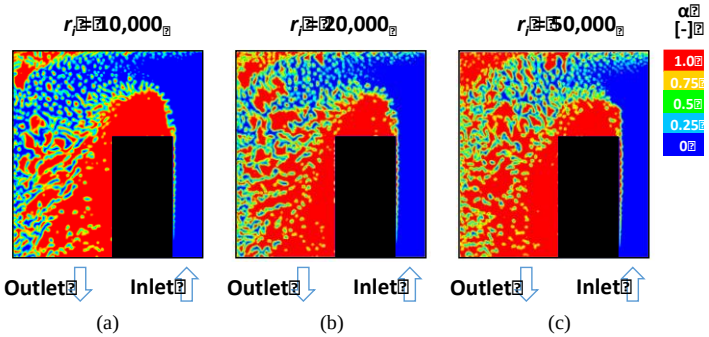

Figure 15 Vapor volume fraction at the center plane of microchannel for three different r_i values of (a) r_i = 10000, (b) r_i = 20000 and (c) r_i = 50000.

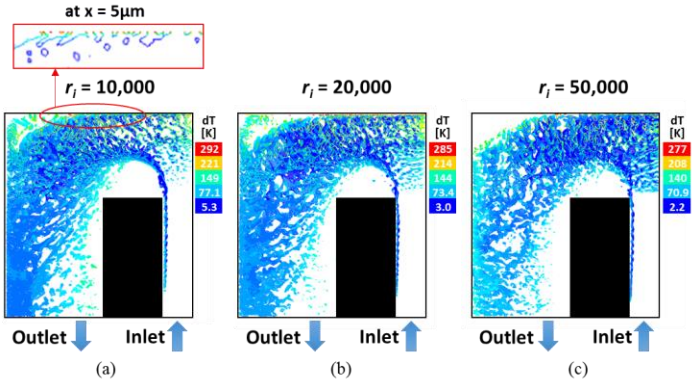

Figure 16 Temperature difference between the local temperature and the saturated temperature at the interface for three different r_i values of (a) r_i = 10000, (b) r_i = 20000 and (c) r_i = 50000.

CONCLUSION

The 3D solid conduction simulation and conjugate CFD simulation models have been performed to predict the microcooler performances for the extreme heat flux GaN HEMT applications. The solid conduction simulation models using COMSOL Multiphysics models account for the overall thermal resistances from GaN HEMT to the microchannel walls. The conjugate CFD simulation models using ANSYS Fluent reveal valuable details on thermofluidic characteristic for both single-phase and two-phase flow of a single-cell configuration. Key findings from the study are as follows.

(1) Solid conduction simulation models evaluate the performance of suggested microcooler design with a broad range of heat transfer coefficients by providing temperature distribution.
(2) Single-phase CFD simulations are conducted to obtain the lower bound of total pressure drop and heat transfer coefficient at the microchannel walls for the mass velocity range of G = 6000 – 24000 kg/m^2-s.
(3) The local temperature and velocity distributions reported from the single-phase CFD help with identifying the approximate locations of the maximum velocity and recirculation regions that are susceptible to dryouts.
(4) The flow boiling is simulated using VOF method by implementing the Lee model. Vapor volume fraction, local temperature, total pressure drop and heat transfer coefficient results are computed for G = 12000 kg/m^2-s using three different values of r_i = 10000 – 50000.

In particular, the future studies should conduct experimental validation for the VOF simulation results and calibrate r_i values to improve heat transfer coefficient predictions. r_i values tested in the study can be updated based on the experimental data instead of checking local temperature difference at the interface.

ACKNOWLEDGMENTS

This material is based upon work supported by the United States Air Force and DARPA under Contract No. FA-8650-13-C-7374. Any opinions, findings and conclusions or recommendations expressed in this material are those of the author(s) and do not necessarily reflect the views of the United States Air Force and DARPA

NOMENCLATURE

Bo	boiling number
C_p	specific heat
COP	coefficient of performance
Co	confinement number
D_h	hydraulic diameter
E	energy per unit mass
F	force
G	mass velocity
g	gravitational acceleration
h	heat transfer coefficient
h_{fg}	latent heat
k	thermal conductivity
P	pressure
Q	energy transfer term
q''	heat flux
r_i	mass transfer intensity factor
S	mass source term
T	temperature
t	time
u	velocity
w	channel width
x	thermodynamic equilibrium quality

Greek Symbols

ρ	density
μ	dynamic viscosity

Subscripts

AF	annular flow regime
CB	coalescing bubble flow regime
eff	effective
ext	external
in	inlet

REFERENCES

[1]. I. Mudawar, Assessment of high-heat-flux thermal management schemes, IEEE Trans. Compon., Package. Manuf. Technol., Part A, 24, 122-141.
[2]. D.B. Tuckerman, R.F.W. Pease, High-performance heat sinking for VLSI, IEEE Electron Device Letters, Vol. EDL2, No. 5, 1981 126-129.
[3]. M. Ohadi, K. Choo, S. Dessiatoun, and E. Cetegen, Force-fed microchannels for high flux cooling applications, in next feneration microchannel heat exchangers, Springer New York, 2013, 33–65.
[4]. S. Scholl, C. Gorle, F. Houshmand, T. Liu, H. Lee, Y. Won, M. Asheghi, K. E. Goodson, H. Kazemi, Numerical simulation of advanced monolithic microcooler designs for high heat flux microelectronics, InterPACK/ICNMM 2015, July 6-9, 2015, San Francisco, CA, USA
[5]. K. M. Dowling, A.J. Suria, Y. Won, A. Shankar, H. Lee, M. Asheghi, K. E. Goodson, D. G. Senesky, Inductive coupled plasma etching of high aspect ratio silicon carbide microchannels for localized cooling. InterPACK/ICNMM 2015, July 6-9, 2015, San Francisco, CA, USA
[6]. H. Lee, I. Park, I. Mudawar, M.M. Hasan, Micro-channel evaporator for space applications – 2. Assessment of predictive tools, *Int. J. Heat Mass Transfer* 77 (2014) 1231-1249.
[7]. F. Houshmand, H. Lee, M. Asheghi, K. E. Goodson, Subcooled flow boiling of methanol in microtubes, in preparation.
[8]. S.M. Kim, I. Mudawar, Universal approach to predicting saturated flow boiling heat transfer in mini/micro-channels – Part II. Two-phase heat transfer coefficient, Int. J. Heat Mass 64 (2013) 1239–1256.
[9]. G.R. Warrier, V.K. Dhir, L.A. Momoda, Heat transfer and pressure drop in narrow rectangular channels, Experimental Thermal Fluid Science 26 (2002) 53–64.
[10]. B. Agostini, A. Bontemps, Vertical flow boiling of refrigerant R134a in small channels, Int. J. Heat Fluid Flow 26 (2005) 296–306.

[11]. H.K. Oh, C.H. Son, Flow boiling heat transfer and pressure drop characteristics of CO_2 in horizontal tube of 4.57-mm inner diameter, Applied Thermal Engng 31 (2011) 163–172.
[12]. A. Cioncolini, J. R. Thome, Algebraic turbulence modeling in adiabatic and evaporating annular two-phase flow, Int. J. Heat Fluid Flow, 32 (2011) 805–817.
[13]. M.M. Shah, Chart correlation for saturated boiling heat transfer: equations and further study, ASHRAE Trans. 88 (1982) 185–196.
[14]. M. Ducoulombier, S. Colasson, J. Bonjour, P. Haberschill, Carbon dioxide flow boiling in a single microchannel – part II: heat transfer, Experimental Thermal Fluid Science 35 (2011) 597–611.
[15]. K.E. Gungor, R.H.S. Winterton, A general correlation for flow boiling in tubes and annuli, Int. J. Heat Mass Transfer 29 (1986) 351–358.
[16]. S.S. Bertsch, E.A. Groll, S.V. Garimella, A composite heat transfer correlation for saturated flow boiling in small channels, Int. J. Heat Mass Transfer 52 (2009) 2110–2118.
[17]. T. Harirchian, S.V. Garimella, Flow regime-based modeling of heat transfer and pressure drop in microchannel flow boiling, Int. J. Heat Mass Transfer 55 (2012) 1246–1260.
[18]. E. Costa-Patry, J. R. Thome, Flow pattern-based flow boiling heat transfer model for microchannels, Int. J. Refrigeration 36 (2013) 414-420.
[19]. W.H. Lee, A pressure iteration scheme for two-phase flow modeling, in: T.N. Veziroglu, ed., Multiphase transport fundamentals, reactor safety, applications, vol. 1, Hemisphere Publishing, Washington, DC, 1980.
[20]. ANSYS FLUENT 12.1 in Workbench User's Guide. ANSYS Inc., Canonsburg, PA, 2009.
[21]. C. R. Charangate, H. Lee, I. Mudawar, Computational Modeling of Turbulent Evaporating Falling Films, *Int. J. Heat Mass Transfer* 81 (2015) 52-62.
[22]. H. Lee, C.R. Kharangate, N. Mascarenhas, Ilchung Park, I. Mudawar, Experimental and Computational Investigation of Vertical Downflow Condensation, *Int. J. Heat Mass Transfer*. 85 (2015) 865–879.
[23]. B. van Leer, Towards the ultimate conservative difference scheme, V. A second order sequel to Godunov's method, J. Computational Physics 32 (1979) 101–136.
[24]. S.V. Patankar, Numerical heat transfer and fluid flow, Hemisphere Publishing, New York, 1980.
[25]. C.W. Hirt, B.D. Nichols, Volume of fluid (VOF) method for the dynamics of free boundary, J. Computational Physics 39 (1981) 201–225.
[26]. D.L. Youngs, Time-dependent multi-material flow with large fluid distortion, Numerical Methods Fluid Dynamics, Academic Press, New York, 1982.